

COMPLETE COMPLEMENTARY SEQUENCE CODING WAVEFORM BASED AZIMUTH MULTI-CHANNEL SPACE-BORNE SAR WITH ULTRA-LOW RANGE SIDELOBE RATIO PERFORMANCE

Jie Chen, Yan Qing Zhu, Peng Bo Wang^{*}, and Wei Yang

School of Electronics and Information Engineering, Beihang University, Beijing 100191, China

Abstract—Sidelobes of strong targets substantially impact image quality of synthetic aperture radar (SAR) using linear frequency modulation (LFM) waveform, especially in urban areas. A novel space-borne azimuth multi-channel SAR scheme with ultra-low range sidelobe-ratio (RSLR) performance was proposed, employing complete complementary sequence (CC-S) coding waveform. The CC-S waveform was utilized to acquire ultra-low RSLR performance in range direction. Azimuth multi-channel scheme was introduced, to compensate reduction of effective PRF due to employing CC-S, and to mitigate azimuth resolution lost resulted from strong azimuth weighting, in order to implement low side-lobe performance in both range and azimuth direction. The method for pre-processing the CC-S based multi-channel SAR data was proposed, which would both compensate receiving time difference of sub-sequences and reconstruct azimuth spectrum of multi-channel SAR data. Furthermore, the corresponding image formation algorithm for accurately focusing raw data of the SAR system was also proposed. Computer simulation results were presented, which demonstrated the validity of the proposed SAR scheme and image formation algorithm.

1. INTRODUCTION

Synthetic aperture radar (SAR) is widely used in microwave remote sensing applications, which has all-time and all-weather earth observation capability [1–6]. Improving SAR image quality becomes more and more significant for current SAR systems [7–8]. Linear

Received 29 May 2013, Accepted 29 July 2013, Scheduled 23 August 2013

* Corresponding author: Pengbo Wang (wangpb7966@163.com).

frequency modulation (LFM) waveform is widely employed as radar transmitted waveform in conventional SAR systems, thus strong sidelobe, due to range compression processing on LFM, inevitably affects SAR image quality [7]. Sidelobes of strong targets, e.g., large buildings, shown as cross-shaped patterns, submerge the neighboring weaker targets, especially in urban areas, thus greatly impact SAR image quality [6–8].

Spectral weighting is one of the traditional sidelobe suppression methods [9], which is widely used at the expense of sacrificing spatial resolution. Meanwhile, some nonlinear algorithms were proposed to reduce sidelobe without significantly compromising spatial resolution, e.g., dual apodization (DA) [7], spatially variant apodization (SVA) [7, 8]. However, such nonlinear methods additionally introduce radiometric artifacts into SAR images [9]. As another solution, phase coding sequences were employed as radar waveforms to reduce range sidelobe ratio (RSLR) [10]. In order to assess performance of phase coding sequences based SAR system, auto-correlation function (ACF) of radar waveform, referred to as SAR impulse response function was investigated. Complete complementary sequence (CC-S) was proposed by Suehiro in 1982 [13]. The CC-S consists of several groups of self-complementary sequences, and each group is also composed of several sub-sequences [11–13]. For each group, the sum for each ACF of respective sub-sequence is ideal impulse function, named as self-complementary property [11, 13].

Unlike general phase coding sequences, a group of self-complementary sequences should be sequentially transmitted and received as respective pulses when used in SAR systems, with one pulse cycle as the interval. As the echo pulses belong to the same group of self-complementary sequences, they should be processed together to acquire ultra-low range RSLR performance. These pulses can be regard as one pulse. Thus the effective PRF reduces to $1/N$ of its original value, where N represents the number of sub-sequences in each group, resulting in limitation on swath width. Besides, strong azimuth weighting process should be carried out on SAR data to reduce azimuth sidelobe, meanwhile inevitably degrading the azimuth resolution. As a result, more margins should be considered in system design. Particularly, PRF is required to be increased. Hence, azimuth multi-channel scheme is adopted to increase effective PRF. By splitting SAR antenna into multiple receive sub-apertures in azimuth direction, the antenna can receive more echo samples for each transmitted pulse, to increase effective PRF [5, 14–17]. The corresponding reconstruction algorithm for reconstructing the azimuth spectrum of multi-channel SAR data was proposed in [14]. In this

paper, the azimuth multi-channel SAR scheme employing CC-S as the SAR transmitted signal was proposed. As each sub-sequence of CC-S is sequentially transmitted, the receiving time difference of sub-sequences should be compensated. Since multi-channel reconstruction processing is also implemented in azimuth direction, these steps can be combined together as the pre-processing step. Then, the whole imaging formation algorithm for accurately focusing the raw data of the SAR system was introduced.

The outline of this paper is arranged as follows. Section 2 introduces the concept of CC-S and derives the pre-processing method of multi-channel SAR using CC-S waveform. Section 3 presents the corresponding imaging formation algorithm. In Section 4, the simulation results are presented. Finally, summary and conclusions are presented in Section 5.

2. CC-S BASED MULTI-CHANNEL SAR SCHEME

2.1. CC-S Phase Coding

CC-S is widely used in communication systems, for its perfect correlation function property. Research on complementary series began in 1960s. At first, the binary complementary series were defined as a pair of equally long sequences consisting of two kinds of elements, and the sum of their two respective autocorrelation series was zero everywhere, except for the zero-shift term [11, 12, 18]. The further concept of complementary series was developed by Tseng and Liu [11, 12, 18], and the multiphase complementary series were derived by Sivaswamy [11, 12, 18]. Based on the previous research, Suehiro extended the concept to families of complete complementary sequence (CC-S) whose auto-correlation is equal to zero for all shifts except zero shift, and the cross-correlation is zero for all shifts [13]. The CC-S has recently renewed interest in the area of high-resolution SAR waveform design due to their ability of perfect sidelobe cancellation.

The CC-S is composed of M groups of self-complementary sequences [18], represented by (1).

$$\begin{cases} \{A_1, A_2, \dots, A_N\} \\ \{B_1, B_2, \dots, B_N\} \\ \{C_1, C_2, \dots, C_N\} \\ \vdots \\ \{M_1, M_2, \dots, M_N\} \end{cases} \quad (1)$$

where one group of the self-complementary sequences $\{A_1, A_2, \dots, A_N\}$

are composed of N sub-sequences with length L , which satisfy [18]

$$R_{A_1}(\tau) + R_{A_2}(\tau) + \dots + R_{A_N}(\tau) = \begin{cases} NL, & \tau = 0 \\ 0, & \tau \neq 0 \end{cases} \quad (2)$$

$$\begin{cases} R_{A_1, B_1}(\tau) + R_{A_2, B_2}(\tau) + \dots + R_{A_N, B_N}(\tau) \equiv 0 \\ R_{A_1, C_1}(\tau) + R_{A_2, C_2}(\tau) + \dots + R_{A_N, C_N}(\tau) \equiv 0 \\ \vdots \\ R_{B_1, A_1}(\tau) + R_{B_2, A_2}(\tau) + \dots + R_{B_N, A_N}(\tau) \equiv 0 \\ R_{B_1, C_1}(\tau) + R_{B_2, C_2}(\tau) + \dots + R_{B_N, C_N}(\tau) \equiv 0 \\ \vdots \\ \vdots \end{cases} \quad (3)$$

where $R_{A_i}(\tau)$ represents the aperiodic auto-correlation function of sub-sequence A_i , and $R_{A_i, B_i}(\tau)$ represents the aperiodic cross-correlation of sub-sequences A_i and B_i . Expressions (2) and (3) mean the self-complementary property and orthogonal property of CC-S, respectively. By using CC-S as transmitted waveform, the SAR system can acquire ultra-low RSLR performance, due to the self-complementary property of CC-S.

For simplicity, only one group of self-complementary sequences of CC-S, which are composed of two sub-sequences, are chosen for analysis and discussion, as shown in (4). The group of self-complementary sequences $\{A_1, A_2\}$ can be yielded by iteration, referring to the construction method of CC-S proposed in [19]. Hence, the expression (2) can be modified as (5) accordingly.

$$\begin{cases} A_1 = (a_1^0, a_1^1, \dots, a_1^{L-1}) \\ A_2 = (a_2^0, a_2^1, \dots, a_2^{L-1}) \end{cases} \quad (4)$$

$$R_{A_1}(\tau) + R_{A_2}(\tau) = \begin{cases} NL, & \tau = 0 \\ 0, & \tau \neq 0 \end{cases} \quad (5)$$

When $\{A_1, A_2\}$ are employed as transmitted waveform, the respective pulses are transmitted alternatively with the same carrier-frequency, thus they can be separated for the posteriori process.

2.2. Multi-channel SAR Scheme Using CC-S

As discussed in Section 1, the azimuth multi-channel SAR scheme, which achieves the time up-sampling by spatially up-sampling, is introduced to increase the effective PRF [20–22].

The receiving antenna of multi-channel SAR can be divided into N receiver sub-apertures in along-track direction, combined with a

single transmitter aperture [20–22]. When SAR sensor works, the transmitter aperture transmits the SAR signal pulses to the ground with the time interval $1/\text{PRF}$, and after the propagating delay, the N receiver apertures receive the reflex signal simultaneously [20–22]. The transmitter or receiver aperture can be represented by a virtual point called phase center, which is the effective position of transmitted or received signal [20–22]. The spacing of adjacent phase center is supposed as d .

Unlike in the conventional SAR system, the SAR signal shares different propagating paths when transmitted and received in the multi-channel SAR system, with the stop-go model. The azimuth impulse response for a point-like target is determined by the total length of propagating paths, which is the summation of transmitting path $R_t(t)$ and receiving path (from ground target to receiver j phase center) $R_{r,j}(t)$, not twice as much as the distance from antenna phase center to the ground target. By assuming a straight sensor trajectory, $R_t(t)$ and $R_{r,j}(t)$ can be written as (6) and (7) [23].

$$R_t(t) = \sqrt{R_0^2 + (v_s \cdot t)^2} \quad (6)$$

$$R_{r,j}(t) = \sqrt{R_0^2 + (v_s \cdot t - d_j)^2} \quad (7)$$

where v_s is the velocity of SAR sensor, R_0 the slant range at the azimuth time $t = 0$, λ the carrier wavelength, and d_j the spacing of transmitter phase center and receiver j phase center.

Considering (6) and (7), the azimuth impulse response of receiver j for a point-like target can be described by (8) [23].

$$\begin{aligned} h_j(t) &= \exp \left\{ -j \frac{2\pi}{\lambda} [R_t(t) + R_{r,j}(t)] \right\} \\ &\approx \exp \left[-j \frac{4\pi}{\lambda} \sqrt{R_0^2 + \left(v_s \cdot t - \frac{d_j}{2} \right)^2} \right] \\ &= \exp \left[-j \frac{4\pi}{\lambda} R_t \left(t - \frac{d_j}{2v_s} \right) \right] \end{aligned} \quad (8)$$

In (8), quadratic approximation is adopted, and a small constant phase shift $\Delta\varphi_j = -\frac{\pi \cdot d_j^2}{2\lambda R_0}$ is ignored. For comparison, the azimuth impulse response for mono-channel SAR is given by

$$h_s(t) = \exp \left[-j \frac{4\pi}{\lambda} R_t(t) \right] \quad (9)$$

According (8) and (9), the multi-channel azimuth impulse response of receiver j can be regarded as the delay of the mono-channel

scenario [23]. Thus, the system function of delay system in azimuth frequency domain (Doppler domain) is derived as (10), considering (8) and (9) [23].

$$H_j(f_t) = \exp\left(-j\frac{\pi \cdot d_j}{v_s} f_t\right) \quad (10)$$

The multi-channel SAR data should be pre-processed before the posterior focusing steps, similar to the mono-channel scenario. The pre-process is also called spectrum reconstruction, which can convert the multi-channel SAR signal into mono-channel SAR signal, based on the linear system theory [14, 23].

Since the received signals are sampled in azimuth by PRF, the compact characterization of the whole multi-channel SAR system can be given by the matrix $\mathbf{H}(f_t)$ shown in (11), which consists of the system function for each channel [14, 23].

$$\mathbf{H}(f_t) = \begin{bmatrix} H_1(f_t) & \dots & H_N(f_t) \\ H_1(f_t + \text{PRF}) & \dots & H_N(f_t + \text{PRF}) \\ \vdots & \ddots & \vdots \\ H_1(f_t + (N-1)\text{PRF}) & \dots & H_N(f_t + (N-1)\text{PRF}) \end{bmatrix} \quad (11)$$

Further, as shown in [10], the inversion of $\mathbf{H}(f_t)$ yields a filter matrix $\mathbf{G}(f_t)$ [14, 23], given by (12).

$$\begin{aligned} \mathbf{G}(f_t) &= N \cdot \mathbf{H}^{-1}(f_t) \\ &= \begin{bmatrix} G_1(f_t) & G_1(f_t + \text{PRF}) & \dots & G_1(f_t + (N-1)\text{PRF}) \\ G_2(f_t) & G_2(f_t + \text{PRF}) & \dots & G_2(f_t + (N-1)\text{PRF}) \\ \vdots & \vdots & \ddots & \vdots \\ G_N(f_t) & G_N(f_t + \text{PRF}) & \dots & G_N(f_t + (N-1)\text{PRF}) \end{bmatrix} \end{aligned} \quad (12)$$

where each row of $\mathbf{G}(f_t)$ represents the “reconstruction filter” for signal of respective channel, and each column represents filter of the respective sub-band with width PRF. Filtered by $\mathbf{G}(f_t)$, multi-channel SAR signal can be equivalent to mono-channel SAR signal, in azimuth frequency domain.

Then, the scenario employing the complete complementary sequence is discussed. Firstly, baseband form of transmitted signal can be described by

$$\begin{cases} s_{A_1}(\tau) = a_1^l, & (l-1) \cdot T_c \leq \tau < l \cdot T_c \quad l = 1, 2, \dots, L \\ s_{A_2}(\tau) = a_2^l, & (l-1) \cdot T_c \leq \tau < l \cdot T_c \quad l = 1, 2, \dots, L \end{cases} \quad (13)$$

where, T_c represents the duration of each code element.

The transmitted pulses of A_1 and A_2 are transmitted alternately, thus the respective receiving time does not coincide, differing with one

pulse repetition interval. The demodulated echo signal of point target can be given as (14) and (15).

$$\begin{aligned}
 & x_1(t_1, \tau) \\
 &= w_a(t_1 - t_0) \cdot \text{rect}\left(\frac{\tau - \tau_1}{t_p}\right) \cdot \exp\{-j2\pi f_c \tau_1\} \cdot s_{A_1}(\tau - \tau_1) \quad (14)
 \end{aligned}$$

$$\begin{aligned}
 & x_2(t_2, \tau) \\
 &= w_a(t_2 - t_0) \cdot \text{rect}\left(\frac{\tau - \tau_2}{t_p}\right) \cdot \exp\{-j2\pi f_c \tau_2\} \cdot s_{A_2}(\tau - \tau_2) \quad (15)
 \end{aligned}$$

where the propagation delay $\tau_1 = \frac{2R(t_1)}{c}$, $\tau_2 = \frac{2R(t_2)}{c}$, t_1 and t_2 are the slow time of echo signal with respect to $s_{A_1}(\tau)$ and $s_{A_2}(\tau)$, and $t_2 = t_1 + \frac{1}{\text{PRF}}$.

After range matched filtering, the output can be written as (16) and (17), respectively.

$$x_{rc1}(t_1, \tau) = w_a(t_1 - t_0) \cdot \exp\{-j2\pi f_c \tau_1\} \cdot R_{A_1}(\tau - \tau_1) \quad (16)$$

$$x_{rc2}(t_2, \tau) = w_a(t_2 - t_0) \cdot \exp\{-j2\pi f_c \tau_2\} \cdot R_{A_2}(\tau - \tau_2) \quad (17)$$

The respective azimuth phase modulations difference between (16) and (17) should be compensated, to satisfy (5). Since the azimuth phase modulations are dependent on target position, the compensation in azimuth time domain is not valid for all the ground targets. Thus the compensation is attempted to be performed in azimuth frequency domain.

Before the azimuth compensation processing, the range compression is performed in range frequency domain. Firstly, range Fourier transform is performed on (14) and (15), deriving (18) and (19), respectively.

$$X_1(t_1, f_\tau) = w_a(t_1 - t_0) \cdot \exp\left\{-j \frac{4\pi(f_c + f_\tau)R(t_1)}{c}\right\} \cdot S_{A_1}(f_\tau) \quad (18)$$

$$X_2(t_2, f_\tau) = w_a(t_2 - t_0) \cdot \exp\left\{-j \frac{4\pi(f_c + f_\tau)R(t_2)}{c}\right\} \cdot S_{A_2}(f_\tau) \quad (19)$$

where $S_{A_1}(f_\tau)$ and $S_{A_2}(f_\tau)$ represent the Fourier transforms of $s_{A_1}(\tau)$ and $s_{A_2}(\tau)$, respectively. By range Fourier transform, each range frequency cell contains full azimuth phase depending on the azimuth time.

Then, the range matched filtering is performed on $X_1(t_1, f_\tau)$ and $X_2(t_2, f_\tau)$ in range frequency domain, without inverse Fourier

transform, and the outputs are given as (20) and (21), respectively.

$$\begin{aligned} & X_{rc1}(t_1, f_\tau) \\ &= w_a(t_1 - t_0) \cdot \exp \left\{ -j \frac{4\pi(f_c + f_\tau)R(t_1)}{c} \right\} \cdot S_{A_1}(f_\tau) \cdot S_{A_1}^*(f_\tau) \quad (20) \end{aligned}$$

$$\begin{aligned} & X_{rc2}(t_2, f_\tau) \\ &= w_a(t_2 - t_0) \cdot \exp \left\{ -j \frac{4\pi(f_c + f_\tau)R(t_2)}{c} \right\} \cdot S_{A_2}(f_\tau) \cdot S_{A_2}^*(f_\tau) \quad (21) \end{aligned}$$

According to (20) and (21), the receiving time difference only exists in azimuth phase terms, which are represented by (22) and (23).

$$s_{a1}(t_1, f_\tau) = w_a(t_1 - t_0) \cdot \exp \left\{ -j \frac{4\pi(f_c + f_\tau)R(t_1)}{c} \right\} \quad (22)$$

$$s_{a2}(t_2, f_\tau) = w_a(t_2 - t_0) \cdot \exp \left\{ -j \frac{4\pi(f_c + f_\tau)R(t_2)}{c} \right\} \quad (23)$$

Azimuth Fourier transform is performed on both $s_{a1}(t_1, f_\tau)$ and $s_{a2}(t_2, f_\tau)$.

$$S_{a1}(f_t, f_\tau) = \int_{-\infty}^{+\infty} s_{a1}(t_1, f_\tau) e^{-j2\pi f_t t_1} dt_1 \quad (24)$$

$$S_{a2}(f_t, f_\tau) = \int_{-\infty}^{+\infty} s_{a2}(t_2, f_\tau) e^{-j2\pi f_t t_2} dt_2 \quad (25)$$

Combining (22)–(25), $S_{a2}(f_t, f_\tau)$ should satisfy (26), and the receiving time difference can be compensated by $\Phi_1(f_t)$.

$$S_{a2}(f_t, f_\tau) = S_{a1}(f_t, f_\tau) \exp\{-j2\pi f_t(t_2 - t_1)\} = S_{a1}(f_t, f_\tau) \cdot \Phi_1(f_t) \quad (26)$$

with

$$\Phi_1(f_t) = \exp \left\{ j2\pi \frac{f_t}{\text{PRF}} \right\} \quad (27)$$

Combining (21), (23) and (25)–(27), the two-dimensional spectrum after compensation can be described as

$$\tilde{X}_{rc2}(f_t, f_\tau) = S_{a1}(f_t, f_\tau) \cdot S_{A_2}(f_\tau) \cdot S_{A_2}^*(f_\tau) \quad (28)$$

According to (20), (22) and (24), $X_{rc1}(f_t, f_\tau)$ can be given by

$$X_{rc1}(f_t, f_\tau) = S_{a1}(f_t, f_\tau) \cdot S_{A_1}(f_\tau) \cdot S_{A_1}^*(f_\tau) \quad (29)$$

By adding $X_{rc1}(f_t, f_\tau)$ and $\tilde{X}_{rc2}(f_t, f_\tau)$, the summation given by (30) consists of two parts. The first part represents the Fourier

transform of azimuth phase modulation, and the second one is the sum for range matched filtering of respective transmitted signals.

$$\begin{aligned} X_{rc}(f_t, f_\tau) &= X_{rc1}(f_t, f_\tau) + \tilde{X}_{rc2}(f_t, f_\tau) \\ &= S_{a1}(f_t, f_\tau) \cdot [S_{A1}(f_\tau) \cdot S_{A1}^*(f_\tau) + S_{A2}(f_\tau) \cdot S_{A2}^*(f_\tau)] \end{aligned} \quad (30)$$

After range inverse Fourier transform is performed on $X_{rc}(f_t, f_\tau)$, the data in range-Doppler domain are similar to the conventional scenario, except for no sidelobe in range direction. For the multi-channel SAR using CC-S, the compensation process for receiving time difference can be combined with the spectrum reconstruction process, by modifying the reconstruction filter. Firstly, the system functions are modified as (31) and (32), respectively.

$$H_{A1,j}(f_t) = \exp\left(-j\frac{\pi \cdot d_j}{v_s} f_t\right) \quad (31)$$

$$H_{A2,j}(f_t) = \exp\left(-j\frac{\pi \cdot d_j}{v_s} f_t\right) \cdot \Phi_1(f_t) \quad (32)$$

Then, (11) and (12) can be modified accordingly.

3. IMAGE FORMATION ALGORITHM

In Section 2, the pre-processing step, i.e., azimuth spectrum reconstruction and compensation of receiving time difference, was introduced. After this step, the echo data belonging to A_1 and A_2 are fused, and the range pulse compression is completed, to acquire the ultra-low sidelobe in range direction. The posteriori process is similar to conventional SAR, i.e., the secondary range compression (SRC), range cell migration correction (RCMC) and azimuth focusing.

Since the implementation of SRC is in the two-dimensional frequency domain by phase multiply, the range inverse Fourier transform is not necessary in range pulse compression.

After the pre-processing, the data in two-dimensional frequency domain can be described by

$$X(f_t, f_\tau) = S_{a1}(f_t, f_\tau) \cdot S_{rc}(f_\tau) \quad (33)$$

where $S_{rc}(f_\tau)$ represents the range Fourier transform of pulse compression of CC-S, and $S_{a1}(f_t, f_\tau)$ is the azimuth spectrum, given by

$$S_{a1}(f_t, f_\tau) = \int_{-\infty}^{+\infty} w_a(t_1 - t_0) \cdot \exp\left\{-j\frac{4\pi(f_c + f_\tau)R(t_1)}{c}\right\} dt_1 \quad (34)$$

Using the hyperbolic form of the range equation and the principle of stationary phase (POSP), $X(f_t, f_\tau)$ can be described by (35), (36), (37) and (38) [24].

$$X(f_t, f_\tau) = W_a(f_t - f_{dc}) \cdot \exp\{j\theta_a(f_t, f_\tau)\} \cdot S_{rc}(f_\tau) \quad (35)$$

$$W_a(f_t) = w_a \left(\frac{-cR_0 f_t}{2(f_0 + f_\tau) V_r^2 \sqrt{1 - \frac{c^2 f_t^2}{4V_r^2(f_0 + f_\tau)^2}}} \right) \quad (36)$$

$$\theta_a(f_t, f_\tau) = -\frac{4\pi R_0 f_0}{c} \sqrt{D^2(f_t, V_r) + \frac{2f_\tau}{f_0} + \frac{2f_\tau^2}{f_0^2}} \quad (37)$$

$$D(f_t, V_r) = \sqrt{1 - \frac{c^2 f_t^2}{4V_r^2 f_0^2}} \quad (38)$$

where R_0 represents the slant range when the radar is closest to the target, and V_r represents the effective radar velocity.

By expanding (37) in a power series of f_τ and keeping the first and second order terms, $\theta_a(f_t, f_\tau)$ can be written as [24]

$$\theta_a(f_t, f_\tau) = -\frac{4\pi R_0 f_0}{c} \left(D(f_t, V_r) + \frac{f_\tau}{f_0 D(f_t, V_r)} - \frac{c^2 f_t^2}{8V_r^2 D^3(f_t, V_r) f_0^4} f_\tau^2 \right) \quad (39)$$

The derivation fails in high squint angles. In (39), the third term is due to the cross coupling between range and azimuth, which represents an additional small quadratic phase modulation in range direction. When the squint angle cannot be ignored, this term should be compensated by an accurate and relatively efficient compensation filter $H_{src}(f_t, f_\tau)$ in two-dimensional frequency domain, called SRC filter, which are given by (40) and (41) [24].

$$H_{src}(f_t, f_\tau) = \exp \left\{ -j\pi \frac{f_\tau^2}{K_{src}(R_0, f_t)} \right\} \quad (40)$$

$$K_{src}(R_0, f_t) = \frac{2V_r^2 f_0^3 D^3(f_t, V_r)}{cR_0 f_t^2} \quad (41)$$

According to the discussion above, the small quadratic phase in range direction, caused by the squint case, only depends on the squint level, is independent of the transmitted waveform. Hence, the SRC filter for the novel SAR scheme proposed in this paper is the same as the conventional case.

After the SRC process, the remainder process steps are the same as the conventional SAR and will not be described in details. The

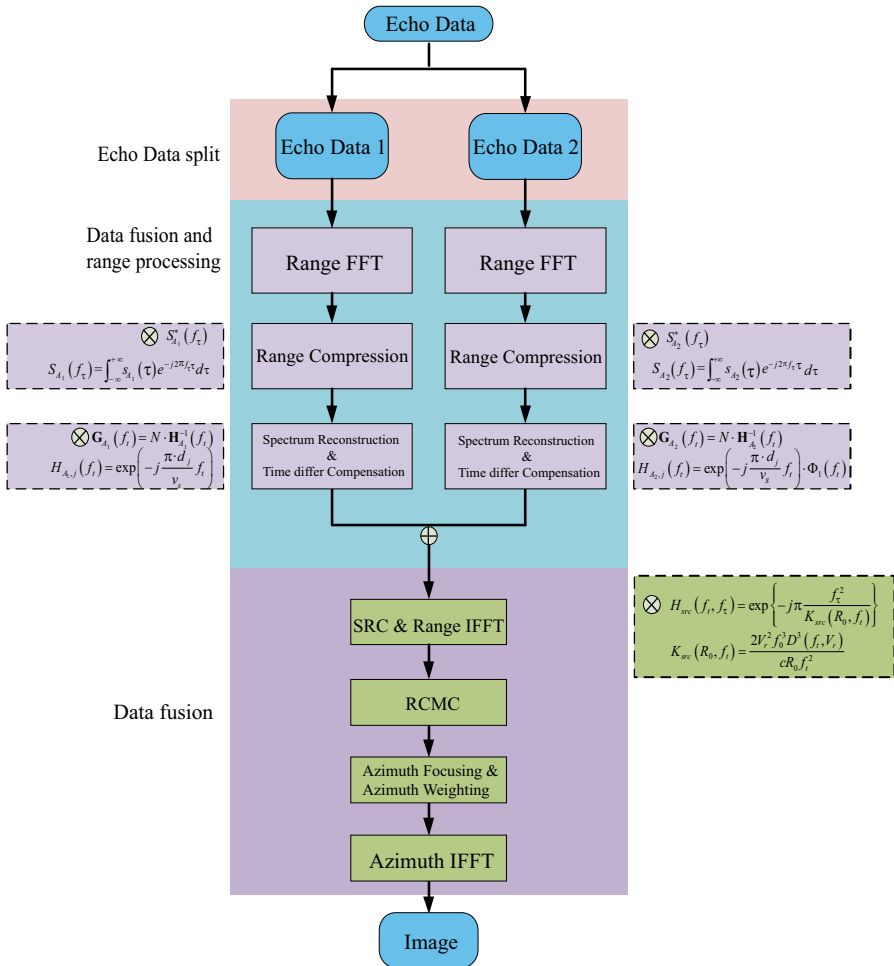


Figure 1. Flowchart of Imaging Algorithm.

flowchart of process algorithm is shown in Figure 1. The Hamming window weighting is included in the flowchart, to reduce the azimuth sidelobe and obtain similar sidelobes in range direction and azimuth direction. Besides, the echo data are divided into two parts, belonging to each sub-sequence, respectively.

Then, the calculated amount of the proposed algorithm will be compared with the conventional SAR image formation algorithm. The comparison is based on the same RDA framework.

In the range pulse compression and azimuth spectral reconstruct-

tion, calculated amount of proposed algorithm is twice as much as the conventional multi-channel SAR. After the data fusion, the calculated amount is the same as the conventional multi-channel SAR. As a result, the calculated amount of proposed algorithm is not more than twice of the conventional multi-channel SAR image formation algorithm.

4. SIMULATIONS

To validate the effectiveness of the proposed multi-channel SAR scheme based on CC-S, simulation experiments were carried out. One group of self-complementary sequences $\{A_0, A_1\}$, given by (4), are applied to the multi-channel SAR system. The transmitted signals with respect to A_1 and A_2 are alternatively transmitted by the transmitter aperture. Key parameters are listed in Table 1.

Table 1. Simulation parameters.

Parameter	Value
Orbit Height	500 km
Elevation Angle	35 deg
Wavelength	0.3 m
SAR Platform Velocity	7725.90 m/s
Slant Range	622.6 km
Antenna Length	15
Number of Receiver	3
Phase Center Interval	5.0 m
Pulse Repetition Frequency	200 Hz
Sampling Rate	200 MHz
Pulse Width	6 μ s
Subsequence Code Length	400
Bandwidth	100 MHz

According to the imaging algorithm proposed in Section 3, the simulated data are processed, including the SAR echo data from nine point targets as shown in Figure 2. The imaging result of SAR based on CC-S is shown in Figure 3(a), and the imaging result of conventional SAR based on LFM is shown in Figure 3(b) for comparison. Figures 3(c) and (d) illustrate the range profile for imaging results of point target based on CC-S and LFM, respectively. The results are listed in Table 2 in detail.

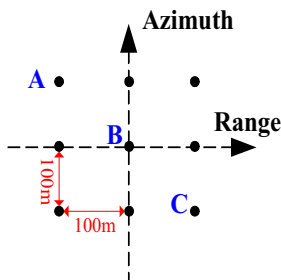


Figure 2. Simulation Scene.

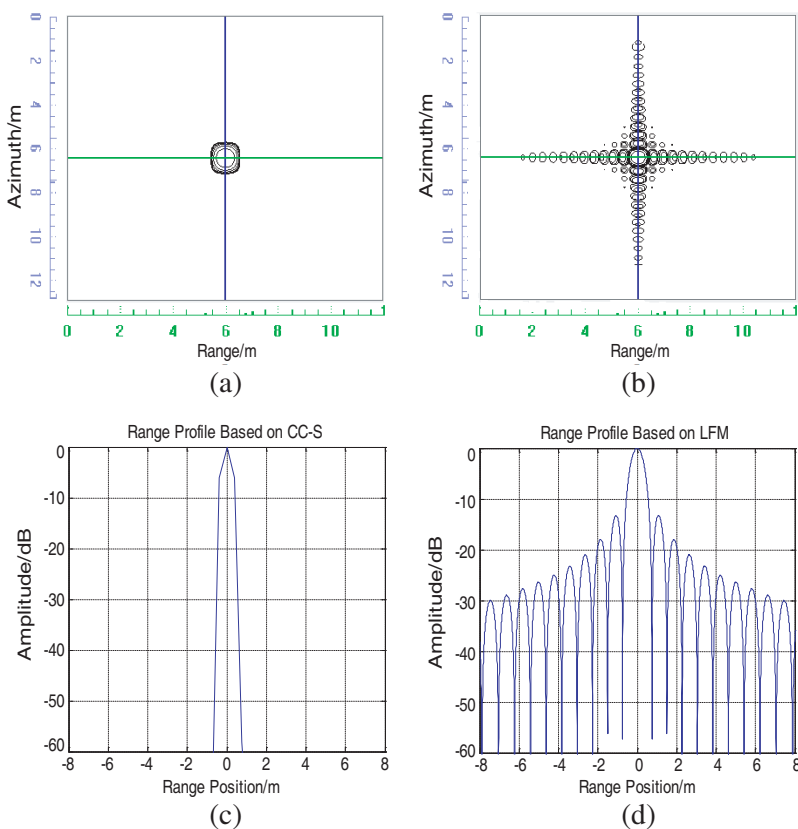


Figure 3. Imaging results of point target. (a) Imaging results based on CC-S. (b) Imaging results based on LFM. (c) Range profile based on CC-S. (d) Range profile based on LFM.

Table 2. Imaging qualities based on CC-S.

Point Number	Resolution(m)		PSLR(dB)	
	Azimuth	Ground Range	Azimuth	Range
1	2854	2.620	-41.705	-78.912
2	2.85	2.617	-41.979	-79.320
3	2.852	2.615	-41.431	-79.123
4	2.85	2.618	-41.854	-79.402
5	2.859	2.617	-41.299	-79.410
6	2.852	2.615	-40.586	-78.891
7	2.853	2.619	-40.500	-79.331
8	2.854	2.617	-41.271	-79.210
9	2.851	2.616	-40.914	-78.740

According to the imaging results, the range PSLR is very low, almost contributed by computer accuracy error. But the range resolution is maintained. In contrast, the azimuth resolution is broadened seriously, when azimuth PSLR is reduced by Hamming window weighting.

Simulation result on distributed scene is also presented here to demonstrate the proposed scheme. The simulated data are generated from the ground scene based on the TerraSAR-X data. Figure 4(a)

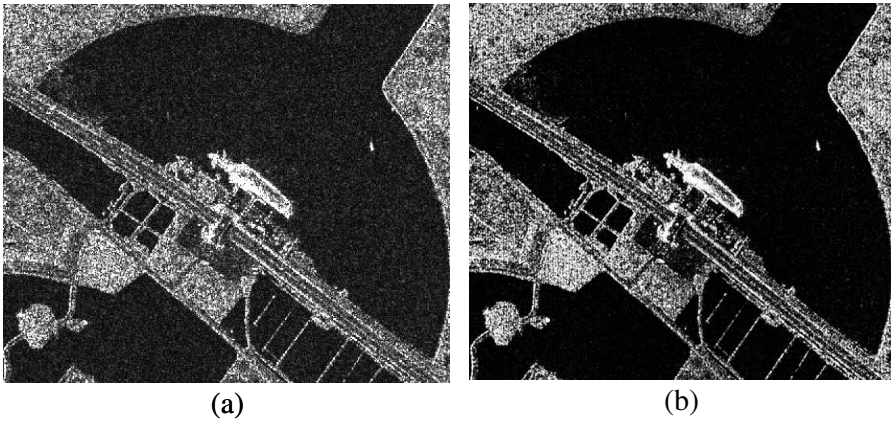


Figure 4. (a) Origin image of the ground scene. (b) Image formation result of simulated data.

is the origin image of the ground scene and Figure 4(b) the image formation result of simulated data.

According to the simulation results on distributed scene, the proposed algorithm is still valid. Besides, the pulse repetition frequency can be reduced by the multi-channel scheme, thus the system design becomes easier.

5. CONCLUSION

This paper presents a novel multi-channel SAR based on CC-S and proposes the corresponding process algorithm. Unlike the conventional SAR system employing the LFM, the SAR system based on CC-S can obtain ultra-low RSLR performance, thus improve the imaging quality. As CC-S consists of a pair of self-complementary sequences, the compensation method has been introduced to compensate the receiving time difference of each sub-sequence. As follow, the compensation method is combined with the multi-channel SAR spectrum reconstruction. At last, the whole imaging algorithm is given. Based on the proposed algorithm, the imaging results reveal a good performance of multi-channel SAR based on CC-S and not only improve the imaging quality, but also reduce the difficulty of system design.

ACKNOWLEDGMENT

This work was supported by the National Natural Science Foundation of China (NSFC) under Grant No. 61132006 and No. 61171123.

REFERENCES

1. Wang, Y., J. Li, J. Chen, H. Xu, and B. Sun, "A novel non-interpolation polar format algorithm using non-linear flight trajectories and auto-adaptive PRF technique," *Progress In Electromagnetics Research*, Vol. 122, 155–173, 2012.
2. Chen, J., J. Gao, Y. Zhu, W. Yang, and P. Wang, "A novel image formation algorithm for high-resolution wide-swath spaceborne SAR using compressed sensing on azimuth displacement phase center antenna," *Progress In Electromagnetics Research*, Vol. 125, 527–543, 2012.
3. Ismail, A., M. Mohamadpoor, R. S. A. Raja Abdullah, and A. F. Abas, "A circular synthetic aperture radar for on-the-

- ground object detection,” *Progress In Electromagnetics Research*, Vol. 122, 269–292, 2012.
4. Sun, J., S. Mao, G. Wang, and W. Hong, “Extended exact transfer function algorithm for bistatic SAR of translational invariant case,” *Progress In Electromagnetics Research*, Vol. 99, 89–108, 2009.
 5. Xu, W., P. P. Huang, and Y. K. Deng, “Multi-channel SPCMB-TOPS SAR for high-resolution wide-swath imaging,” *Progress In Electromagnetics Research*, Vol. 116, 533–551, 2011.
 6. Zhang, M., Y. W. Zhao, H. Chen, and W. Q. Jiang, “SAR imaging simulation for composite model of ship on dynamic ocean scene,” *Progress In Electromagnetics Research*, Vol. 113, 395–412, 2011.
 7. Stankwitz, H. C., R. J. Dallaire, and J. R. Fienup, “Spatially variant apodization for sidelobe control in SAR imagery,” *Radar Conference*, 132–137, 1994.
 8. Thomas, G., B. C. Flores, and J. Sok-Son, “SAR sidelobe apodization using the Kaiser window,” *Imaging Processing*, 709–712, 2000.
 9. Zhang, P., Z. Li, J. Zhou, and Q. Chen, “A new SAR superresolution imaging algorithm based on adaptive sidelobe reduction,” *Proc. IGARSS*, 2789–2792, Toronto, Canada, 2011.
 10. Li, S. F., J. Chen, L. Q. Zhang, and Y. Q. Zhou, “Image formation algorithm for missile borne MMW SAR with phase coded waveform,” *Proc. Radar Conference*, 1–4, 2009.
 11. Durai, R. S. R., “A class of optimal complete-complementary codes of different length,” *Proc. Signal Design and Its Applications in Communications*, 92–95, 2011.
 12. Huang, X. and Y. Li, “Polyphase scalable complete complementary sets of sequences,” *The 8th International Conference on Communication Systems*, Vol. 2, 810–814, 2002.
 13. Suehiro, N., “Complete complementary code composed of N-multiple-shift orthogonal sequences,” *IEICE Trans.*, Vol. J65-A, 1247–1253, 1982.
 14. Gerhard, K., G. Nicolas, and M. Alberto, “Unambiguous SAR signal reconstruction from nonuniform displaced phase center sampling,” *IEEE Geoscience and Remote Sensing Letters*, Vol. 1, No. 4, 260–264, Oct. 2004.
 15. Chua, M. Y. and V. C. Koo, “FPGA-based chirp generator for high resolution UAV SAR,” *Progress In Electromagnetics Research*, Vol. 99, 71–88, 2009.

16. Wei, S. J., X. L. Zhang, J. Shi, and G. Xiang, "Sparse reconstruction for SAR imaging based on compressed sensing," *Progress In Electromagnetics Research*, Vol. 109, 63–81, 2010.
17. Mao, X., D. Y. Zhu, and Z. D. Zhu, "Signatures of moving target in polar format spotlight SAR image," *Progress In Electromagnetics Research*, Vol. 92, 47–64, 2009.
18. Han, C., N. Suehiro, and T. Hashimoto, "N-shift cross-orthogonal sequences and complete complementary Codes," *ISIT 2007*, 2611–2615, Jun. 2007.
19. Li, S., J. Chen, L. Zhang, and Y. Zhou, "Construction of quadri-phase complete complementary pairs applied in MIMO radar systems," *The 9th International Conference on Signal Processing (ICSP)*, 2298–2301, 2008.
20. Currie, A. and M. A. Brown, "Wide-swath SAR," *Proc. Inst. Electr. Eng. F — Radar Signal Process.*, Vol. 139, No. 2, 122–135, Apr. 1992.
21. Gebert, N., G. Krieger, and A. Moreira, "Multichannel azimuth processing in ScanSAR and TOPS mode operation," *IEEE Trans. Geosci. Remote Sens.*, Vol. 48, No. 7, 2994–3008, Jul. 2010.
22. Xu, W. and Y. Deng, "Multi-channel SAR system with reflector antenna for high-resolution wide-swath imaging," *IEEE Antenna and Wireless Propa. Lett.*, Vol. 9, 1123–1126, Dec. 2010.
23. Gebert, N., G. Krieger, and A. Moreira, "Digital beam forming on receive-techniques and optimization strategies for high resolution wide-swath SAR imaging," *IEEE Transaction on Aerospace and Electronic Systems*, Vol. 45, No. 2, 564–592, Apr. 2009.
24. Cumming, I. G. and F. H. Wong, *Digital Processing of Synthetic Aperture Radar Data: Algorithm and Implementation*, Artech House, Norwood, MA, 2005.